Computational and Structural Biotechnology Journal 20 (2022) 3322–3335

COMPUTATIONAL ANDSTRUCTURAL BIOTECHNOLOGY JOURNAL

journal homepage: www.elsevier.com/locate/csbj

Identifies microtubule-binding protein *CSPP1* as a novel cancer biomarker associated with ferroptosis and tumor microenvironment

Wenwen Wang, Jingjing Zhang, Yuqing Wang, Yasi Xu, Shirong Zhang *

Translational Medicine Research Center, Key Laboratory of Clinical Cancer Pharmacology and Toxicology Research of Zhejiang Province, Affiliated Hangzhou First People's Hospital, Zhejiang University School of Medicine, Cancer Center, Zhejiang University, Hangzhou, China

ARTICLE INFO

Article history:
Received 24 April 2022
Received in revised form 19 June 2022
Accepted 21 June 2022
Available online 24 June 2022

Keywords:
CSPP1
Biomarker
Ferroptosis
Tumor microenvironment
Pan-cancer

ABSTRACT

Centrosome and spindle pole-associated protein (*CSPP1*) is a centrosome and microtubule-binding protein that plays a role in cell cycle-dependent cytoskeleton organization and cilia formation. Previous studies have suggested that *CSPP1* plays a role in tumorigenesis; however, no pan-cancer analysis has been performed. This study systematically investigates the expression of *CSPP1* and its potential clinical outcomes associated with diagnosis, prognosis, and therapy. *CSPP1* is widely present in tissues and cells and its aberrant expression serves as a diagnostic biomarker for cancer. *CSPP1* dysregulation is driven by multi-dimensional mechanisms involving genetic alterations, DNA methylation, and miRNAs. Phosphorylation of CSPP1 at specific sites may play a role in tumorigenesis. In addition, *CSPP1* correlates with clinical features and outcomes in multiple cancers. Take brain low-grade gliomas (LGG) with a poor prognosis as an example, functional enrichment analysis implies that *CSPP1* may play a role in ferroptosis and tumor microenvironment (TME), including regulating epithelial-mesenchymal transition, stromal response, and immune response. Further analysis confirms that *CSPP1* dysregulates ferroptosis in LGG and other cancers, making it possible for ferroptosis-based drugs to be used in the treatment of these cancers. Importantly, *CSPP1*-associated tumors are infiltrated in different TMEs, rendering immune checkpoint blockade therapy beneficial for these cancer patients. Our study is the first to demonstrate that *CSPP1* is a potential diagnostic and prognostic biomarker associated with ferroptosis and TME, providing a new target for drug therapy and immunotherapy in specific cancers.

1. Introduction

Cancer is a leading cause of global health problems [1]. Although cancer treatment methods have recently improved, clinical outcomes remain unsatisfactory due to side effects and drug resistance issues. Therefore, it is urgent to identify new sensitive biomarkers for the diagnosis and treatment of these cancer patients.

Abbreviations: TME, tumor microenvironment; CAF, cancer-associated fibroblasts; EMT, epithelial-mesenchymal transition; *CSPP1*, centrosome and spindle pole-associated protein; DLBC, diffuse large B-cell lymphoma; TCGA, The Cancer Genome Atlas; GTEx, Genotype-Tissue Expression; CPTAC, Clinical Proteomic Tumor Analysis Consortium; ROC, receiver operating characteristics; CNA, copy number alteration; KM, Kaplan-Meier; OS, overall survival; DSS, disease-specific survival; PFS, progression-free survival; ENCORI, Encyclopedia of RNA Interactomes; TISIDB, Tumor-Immune System Interactions DataBase; LGG, low-grade gliomas; PFI, progression-free interval; C-index, concordance index; DEGs, differentially expressed genes; GO, Gene Ontology; CC, cellular component; MF, molecular functions; BP, biological pathways; GSEA, Gene Set Enrichment Analysis; KEGG, Kyoto Encyclopedia of Genes and Genomes; GSVA, gene set variation analysis; TIMER, Tumor Immune Estimation Resource; MHC, major histocompatibility complex; TMB, tumor mutation burden; MSI, microsatellite instability; TIDE, Tumor Immune Dysfunction and Exclusion; CTL, cytotoxic T lymphocyte; ICB, immune checkpoint blockade; TGCT, testicular germ cell tumors, STAD, stomach adenocarcinoma; BRCA, breast invasive carcinoma; CHOL, cholangiocarcinoma; COAD, colon adenocarcinoma; ESCA, esophageal carcinoma; GBM, glioblastoma multiforme; HNSC, head and neck squamous cell carcinoma; LAML, acute myeloid leukemia; LIHC, liver hepatocellular carcinoma; PAAD, pancreatic adenocarcinoma; READ, rectum adenocarcinoma; THYM, thymoma; ACC, adrenocortical carcinoma; CESC, cervical squamous cell carcinoma and endocervical adenocarcinoma; KICH, kidney chromophobe; KIRC, renal clear cell carcinoma; LUAD, lung adenocarcinoma; LUSC, lung squamous cell carcinoma; OV, ovarian serous cystadenocarcinoma; PRAD, prostate cancer; SKCM, skin cutaneous melanoma; THCA, thyroid cancer; UCEC, endometrial cancer uterine corpus endometrial carcinoma; UCS, uterine carcinosarcoma; FAG, ferroptosis-associated gene; FDG, ferroptosis-driver gene; FSG, ferroptosis-suppressor gene.

* Corresponding author.
E-mail address: shirleyz4444@zju.edu.cn (S. Zhang).

https://doi.org/10.1016/j.csbj.2022.06.046
2001-0370/

Ferroptosis is a novel iron-dependent programmed cell death, that differs from typical cell death processes, mediated by lethal accumulation of lipid peroxides [2,3]. It involves a series of metabolic pathways and lipid peroxidation signaling pathways and is characterized by increased lipid peroxidation and reactive oxygen species, smaller mitochondria, and higher mitochondrial membrane density, but the change in nuclear morphology is not obvious [4]. Ferroptosis is essentially an antitumor mechanism that suppresses tumor growth and kills these cells. Cancer cell ferroptosis not only promotes the antitumor response of immune cells but also affects the ferroptosis of immune cells themselves. Therefore, ferroptosis plays an important role in tumor occurrence, progression, and prognosis [5,6].

Tumor microenvironment (TME) is the surrounding microenvironment for tumor cells, mainly including peripheral blood vessels, stromal cells (cancer-associated fibroblasts (CAFs), endothelial cells, etc.), immune cells, and non-cellular components (cytokines, growth factors, hormones, and the extracellular matrix) [7–10]. Stromal components typically form a microenvironment conducive to tumor cell growth, including influencing metabolic pathways, inhibiting ferroptosis, inducing epithelial-mesenchymal transition (EMT), and regulating immune cell infiltration. Meanwhile, in the early stage, immune cells are recruited and activated by tumor cells to form an antitumor immune microenvironment and delay tumor development. With the continuous activation by tumor antigens, the relevant effector cells enter the depletion or remodeling stage, resulting in an immunosuppressive microenvironment. Different microenvironmental components interact and regulate each other, and are closely related to tumor progression and prognosis. Therefore, novel targets and biomarkers can be identified by identifying genes that influence ferroptosis and TME, leading to the selection of effective drugs and immunotherapy strategies to improve the prognosis of cancer patients.

Centrosome and spindle pole-associated protein (*CSPP1*), encoded by chromosome 8q13.2, is initially identified as a highly expressed proto-oncogene in diffuse large B-cell lymphoma (DLBC) [11]. It localizes to the interphase centrosome and mitotic spindle, migrates to the central spindle at the end of mitosis, and concentrates at the midbody during telophase and cytokinesis, thus functioning throughout cell cycle progression. Overexpression or suppression of *CSPP1* causes cell-cycle defects [11–14]. Interestingly, CSPP1 is not only localized to the centrosome and spindle in cycling cells but also interacts with Nephrocystin 8 to extend to the cilia axoneme in postmitotic resting cells, thus playing an important role in ciliogenesis. E3 ubiquitin-protein ligase UBR5-mediated ubiquitylation of CSPP1 is an underlying requirement for cilia localization. Meanwhile, interacting with the centrosomal protein of 104 kDa (*CEP104*), CSPP1 regulates axoneme length and cilia formation in the Hedgehog signaling pathway [15–17]. Mutation or loss of function in *CSPP1* causes primary cilia abnormalities and ciliopathy, including Joubert syndrome and Meckel-Gruber syndrome [18–22]. Beyond cell cycle control and ciliogenesis, CSPP1 displays microtubule-independent but desmoplakin-dependent desmosome localization in apical-basal polarized epithelial cells and it is necessary for normal spheroid formation [23]. More importantly, *CSPP1* has also been identified as a candidate oncogene in luminal breast cancer; meanwhile, nuclear *CSPP1* expression can define subtypes and clinical subgroups of basal-like breast carcinoma [24]. In addition to DLBC, *CSPP1* is also identified as a putative hallmark gene associated with the malignancy of oral squamous cell carcinoma [25]. However, no comprehensive analyses of the expression, function, and clinical significance of *CSPP1* as well as its correlation with ferroptosis and TME components have been performed.

In this study, we systematically analyzed *CSPP1* expression and found that its aberrant expression is driven by genetic alterations, DNA methylation, and miRNAs. Phosphorylation of CSPP1 protein may regulate its activity, especially at Ser424. In addition, *CSPP1* strongly correlated with ferroptosis and TME components, potentially serving as a diagnostic and prognostic biomarker. Patients with *CSPP1*-associated tumors may benefit from ferroptosis-based drug therapy and immunotherapy by modulating ferroptosis and TME in several types of cancer.

2. Material and methods

2.1. Data collection

Transcriptomic data containing mRNA, miRNA, and associated clinical information were retrieved from The Cancer Genome Atlas (TCGA, https://portal.gdc.cancer.gov/repository) and UCSC XENA (https://xenabrowser.net) databases [26]. mRNA sequencing data in level 3 HTSeq-FPKM format was converted into TPM format, and miRNA sequencing data in level 3 BCGSC format was converted into RPM format; all data were downloaded from TCGA. UCSC XENA database contained both TCGA and Genotype-Tissue Expression (GTEx) data, which were processed by the Toil process into TPM format [27]. The Oncomine (https://www.oncomine.org/resource/login.html) image for *CSPP1* expression was downloaded (threshold: $p < 0.0001$; fold change >2; gene rank: top 10%). R software (Version 3.6.3, https://cran.r-project.org/bin/windows/base/old/3.6.3/) and ggplot2 R package (Version 3.3.3, https://cran.r-project.org/web/packages/ggplot2/index.html) were used to statistical analyses and visualization, respectively.

2.2. Differential expression analysis

RNA sequencing data in TPM or FPKM format for *CSPP1* expression in tissues and single cells were recorded from the Human Protein Atlas portal (HPA, https://www.proteinatlas.org/) and visualized by radar plots. To compare *CSPP1* and miRNA expression in normal and tumor tissues, an unpaired Wilcoxon rank-sum test was performed using TCGA and GTEx datasets. Histograms of CSPP1 protein expression and site phosphorylation levels in normal and primary tumor tissues were downloaded from the UALCAN portal (https://ualcan.path.uab.edu/analysis-prot.html) using Clinical Proteomic Tumor Analysis Consortium (CPTAC) data [28].

2.3. Diagnostic analysis

The diagnostic value of *CSPP1* was estimated using RNA-sequencing data from TCGA and visualized by a receiver operating characteristics (ROC) curve using the pROC R package (Version 1.17.0.1, https://cran.r-project.org/web/packages/pROC/index.html).

2.4. Genetic alterations and DNA methylation analysis

Histograms of *CSPP1* mutation and copy number alteration (CNA) frequency in pan-cancer (TCGA, PanCancer Atlas) were downloaded from the cBioPortal (https://www.cbioportal.org/). Histograms of *CSPP1* promoter methylation in normal and primary tumor tissues were downloaded from the UALCAN portal (https://ualcan.path.uab.edu/index.html) [29]. Correlations between *CSPP1*, CNAs, and DNA methylation (TCGA, Firehose) were recorded from cBioPortal and visualized by heatmaps. Dot size together with transition color represented the degree of correlation. The larger the dot, the stronger the correlation. Red and blue dots represented positive and negative correlations, respectively. Kaplan-Meier (KM) plots of these alterations on survival probability, including

that of overall survival (OS), disease-specific survival (DSS), and progression-free survival (PFS), were downloaded from cBioPortal.

2.5. Correlations between CSPP1 and associated miRNAs

Spearman correlations between *CSPP1* and associated miRNAs were recorded from the Encyclopedia of RNA Interactomes portal (ENCORI, https://rna.sysu.edu.cn/encori/index.php) (parameter setting: assembly, hg38; miRNA: all; CLIP-Data $\geq$ 3; pan-Cancer $\geq$ 1; programNum $\geq$ 2; target, *CSPP1*) and visualized by a heatmap [30].

2.6. Correlations between CSPP1 and clinical features

Correlations between *CSPP1*, pathologic stage, and histologic grade from TCGA database were analyzed using the Kruskal-Wallis test and visualized by violin plots. Correlations between *CSPP1* and molecular subtype were also analyzed with the Kruskal-Wallis test and the violin plots were downloaded from Tumor-Immune System Interactions DataBase (TISIDB, https://cis.hku.hk/TISIDB/index.php) [31].

Correlations between *CSPP1* and clinical features in brain low-grade gliomas (LGG) were analyzed using the Chi-squared test or Fisher's exact test and visualized by a baseline datasheet.

2.7. Prognostic analysis of CSPP1 and associated miRNAs, model construction, and evaluation

Survival differences analyses of *CSPP1* and associated *miRNAs*, including OS, DSS, and progression-free interval (PFI), were visualized by forest plots based on KM analyses. The Survivin R package (Version 3.2-10, https://cran.r-project.org/web/packages/survivalAnalysis/index.html) was used for statistical analysis, and the survminer R package (Version 0.4.9, https://cran.r-project.org/web/packages/survminer/index.html) was used for visualization.

Univariate and multivariate Cox regression analyses were visualized by forest plots. Based on multivariate Cox regression, risk score plots were constructed using the ggrisk R package (Version 1.3, https://cran.r-project.org/web/packages/ggrisk/index.html). Nomograms were also designed using the rms R package (Version 6.2-0, https://cran.r-project.org/web/packages/rms/index.html) and survival R package [26]. Calibration curves and the concordance index (C-index) were evaluated by comparing predicted probabilities with observed events.

2.8. Functional enrichment analysis in LGG

CSPP1-associated differentially expressed genes (DEGs) in LGG were identified using the limma R package (Version 3.40.2, https://bioconductor.org/packages/release/bioc/html/limma.html) and visualized by a volcano plot [32]. Spearman correlations between *CSPP1* and the top 20 DEGs were assessed and visualized by a heatmap.

DEGs were used for Gene Ontology (GO) enrichment analyses, including cellular components (CCs), molecular functions (MFs), and biological pathways (BPs). Gene Set Enrichment Analysis (GSEA) was also conducted to detect phenotypes and signaling pathways. Hallmark v7.2, GO c5 v7.2 (BPs, CCs, MFs), and Kyoto Encyclopedia of Genes and Genomes (KEGG) c2 v7.2 gene sets were used. Statistical analysis and graphical charting were performed using the clusterProfiler R package (Version 3.14.3, https://bioconductor.org/packages/release/bioc/html/clusterProfiler.html) [32,33].

2.9. Gene mutation and ferroptosis correlation analysis

Somatic mutations in LGG from TCGA database were analyzed using the maftools R package (Version 3.14, https://bioconductor.org/packages/release/bioc/html/maftools.html) and visualized by an oncoplot [34,35]. Ferroptosis-associated score was calculated with the gene set extracted from KEGG with the ssGSEA algorithm in the gene set variation analysis (GSVA) package (Version 1.34.0, https://bioconductor.riken.jp/packages/3.0/bioc/html/GSVA.html), and the difference between the driver score minus suppressor score was defined as the ferroptosis score to represent the ferroptosis status of samples [36]. Spearman correlations between *CSPP1* and ferroptosis-related genes and ferroptosis scores were analyzed and visualized by heatmaps.

2.10. TME analysis and immune checkpoint blockade therapy prediction

TCGA datasets were used to analyze the Spearman correlations between *CSPP1* and immune cells using the ssGSEA algorithm in the GSVA package. They were also used to estimate the stromal score, immune score, and ESTIMATE score using the ESTIMATE package (Version 1.0.13, https://bioinformatics.mdanderson.org/estimate/index.html) [37,38]. Purity-adjusted Spearman correlations between *CSPP1* and CAFs, endothelial cells, and immune checkpoints were recorded from the Tumor Immune Estimation Resource 2 portal (TIMER2, https://timer.cistrome.org) with XCELL or TIMER algorithm [39,40]. The Spearman correlations between *CSPP1* and major histocompatibility complex (MHC) molecules, immune stimulator genes, immune inhibitor genes, tumor mutation burden (TMB) score, and microsatellite instability (MSI) score from the TCGA database were analyzed [41,42]. All corresponding correlations were visualized by heatmaps.

Tumor Immune Dysfunction and Exclusion (TIDE, https://tide.dfci.harvard.edu/) is a comprehensive score for tumor immune dysfunction and immune escape, including tumor-infiltrating cytotoxic T lymphocyte (CTL) dysfunction and rejection by immune checkpoints. RNA-sequencing raw count data and corresponding clinical information from TCGA database were estimated using the TIDE algorithm to predict the potential immune checkpoint blockade (ICB) response. A low score indicated good efficacy [43,44].

3. Results

3.1. Aberrant expression of CSPP1 serves as a diagnostic biomarker among cancers

CSPP1 was widely present in all the tested tissues and cells. It was highly expressed in skeletal muscle, testis, and fallopian tube, as well as in respiratory ciliated cells, endometrial ciliated cells, and early spermatids; meanwhile, high expression was observed in testicular germ cell tumors (TGCT), stomach adenocarcinoma (STAD), and breast invasive carcinoma (BRCA) (Fig. 1A–C).

To compare *CSPP1* expression in human adjacent normal versus 33 types of tumor tissues, TCGA datasets were used. *CSPP1* was significantly upregulated in ten cancer types and downregulated in five from TCGA (Fig. 1D). In order to expand the sample size, we also introduced normal samples from the GTEx database. *CSPP1* expression was increased in BRCA, cholangiocarcinoma (CHOL), colon adenocarcinoma (COAD), DLBC, esophageal carcinoma (ESCA), glioblastoma multiforme (GBM), head and neck squamous cell carcinoma (HNSC), acute myeloid leukemia (LAML), LGG, liver hepatocellular carcinoma (LIHC), pancreatic adenocarcinoma (PAAD), rectum adenocarcinoma (READ), STAD, and thymoma

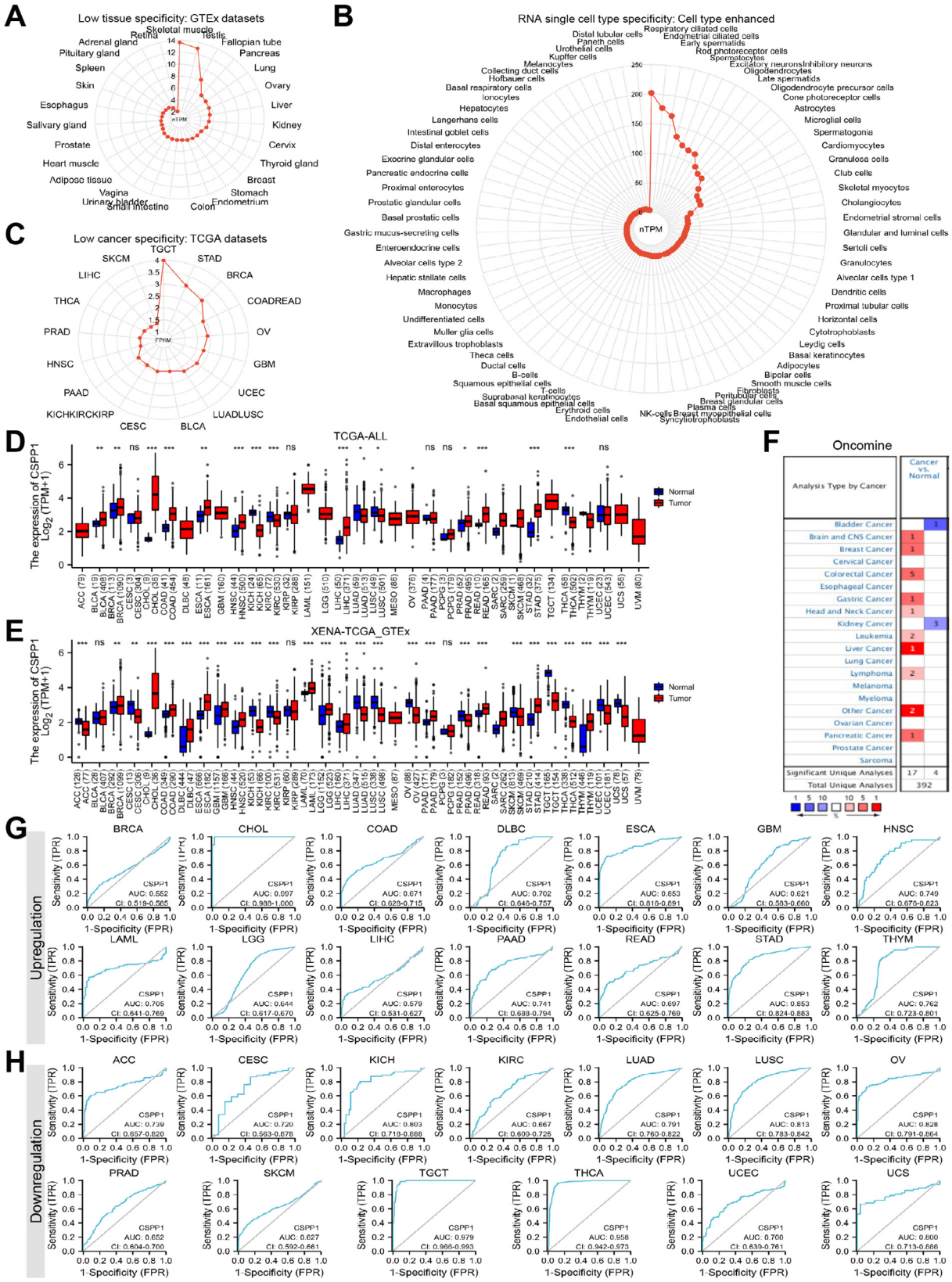

Fig. 1. Aberrant expression of *CSPP1* serves as a diagnostic biomarker among cancers. (A) Radar Plot of *CSPP1* expression in normal tissues basedon GTEx datasets from HPA portal. (B) Radar Plot of *CSPP1* expression in single cells based on single-cell types dataset from HPA portal. (C) Radar Plot of *CSPP1* expression in tumor tissues based on TCGA dataset from HPA portal. (D, E) Histogram of *CSPP1* expression in 33 types of unpaired normal and tumor tissues from TCGA and TCGA plus GTEx database using Wilcoxon rank-sum test. ns: $p \geq 0.05$, * $p < 0.05$, ** $p < 0.01$, *** $p < 0.001$. (F) Heatmap of *CSPP1* expression from Oncomine portal. (G, H) ROC analyses of differential *CSPP1* expression in 27 types of upregulated (G) and downregulated (H) cancer from TCGA and GTEx databases. AUC > 0.9 was considered a high diagnostic value, 0.9 ≥ AUC > 0.7 was median, and 0.7 ≥ AUC > 0.5 was low.

(THYM). In contrast, its expression was decreased in adrenocortical carcinoma (ACC), cervical squamous cell carcinoma and endocervical adenocarcinoma (CESC), kidney chromophobe (KICH), renal clear cell carcinoma (KIRC), lung adenocarcinoma (LUAD), lung squamous cell carcinoma (LUSC), ovarian serous cystadenocarcinoma (OV), prostate cancer (PRAD), skin cutaneous melanoma (SKCM), TGCT, thyroid cancer (THCA), endometrial cancer uterine corpus endometrial carcinoma (UCEC), and uterine carcinosarcoma (UCS) (Fig. 1E). Thereafter, we used the Oncomine datasets to validate *CSPP1* expression patterns. Significantly elevated *CSPP1* expression was observed in most cancer types; however, its expression was reduced in bladder cancer and kidney cancer (Fig. 1F). Combined with these databases, 27 cancers with differential *CSPP1* expression from GTEx plus TCGA database were used in subsequent analyses.

ROC analyses with TCGA or TCGA plus GTEx datasets indicated that the diagnostic values of *CSPP1* were median or high in CHOL, DLBC, ESCA, HNSC, LAML, PAAD, STAD, THYM, ACC, CESC, KICH, LUAD, LUSC, OV, TGCT, THCA, and UCS (Fig. 1G, H). Our results indicated that aberrant *CSPP1* expression serves as a diagnostic biomarker among cancers.

3.2. Multi-dimensional mechanisms involving genetic alterations, DNA methylation, and miRNAs underly CSPP1 dysregulation

To determine the cause underlying *CSPP1* dysregulation, we comprehensively analyzed the factors related to the expression of *CSPP1*, including genetic variation, DNA methylation, and associated miRNAs. We first used cBioPortal to study the genetic variation and found that among these 26 cancer types (COAD and READ were combined into COADREAD in the Portal), 21 contained mutations and 21 had CNAs (Fig. 2A). Except for UCEC (>5%), *CSPP1* mutation frequencies were relatively low in most cancers (<5%). These mutations caused poor PFS in SKCM and good PFS in UCEC (Fig. S1A). CNA is the genetic variation most closely associated with *CSPP1* expression [45]. It occurred more frequently in UCS, PRAD, LIHC, BRCA, and OV (>5%). *CSPP1* positively correlated with CNAs (Fig. 2B; Table S1) and had worse DSS and PFS in COADREAD, as well as worse OS, DSS, and PFS in PAAD, PRAD, STAD, and UCEC (Fig. S1B).

Besides CNAs, DNA methylation also affects gene expression [46]. Promoter methylation was reduced with upregulated *CSPP1* expression in BRCA, HNSC, and READ, while it was increased with downregulated *CSPP1* expression in KIRC and LUSC from UALCAN portal (Fig. 2C; Fig. S2). *CSPP1* expression negatively correlated with DNA methylation from cBioPortal (Fig. 2D and Table S2).

In addition to CNAs and DNA methylation, miRNAs also play important roles in regulating mRNA expression [47]. The ENCORI portal was used to search for miRNAs negatively associated with *CSPP1*. These miRNAs were found in most cancers except for ACC (Fig. 2E; Table S3). We further conducted differential expression analyses of these miRNAs across 14 cancers with data using TCGA datasets. *CSPP1* upregulation was associated with the downregulation of miR-221-3p and miR-377-3p in BRCA; miR-145-5p and miR-125b-5p in STAD (Fig. 2F). Meanwhile, *CSPP1* downregulation may be affected by upregulation of miR-222-3p in KICH; miR-425-5p, miR-221-3p, miR-222-3p, miR-340-5p, miR-150-5p, miR-708-5p in KIRC; miR-135b-5p, miR-222-3p, miR-27a-3p, miR-708-5p in LUAD; miR-135b-5p in LUSC; miR-135a-5p in PRAD; miR-105-5p, miR-221-3p and miR-222-3p in THCA; miR-135b-5p and miR-27a-3p in UCEC (Fig. 2G). A prognosis-related forest plot indicated that in *CSPP1*-overexpressed cancers, downregulated miR-221-3p in BRCA caused favorable DSS and PFI; meanwhile, downregulated miR-145-5p and miR-125-5p in STAD had favorable OS, DSS, and PFI. Among cancers with low *CSPP1* expression, upregulated miR-425-5p, miR-221-3p, miR-222-3p, and miR-708-5p in KIRC caused poor OS, DSS, and PFI; whereas, upregulated miR-27a-3p in LUAD had poor OS and DSS (Fig. 2H; Fig. S3). Together, *CSPP1* dysregulation involves multi-dimensional mechanisms, including genetic alterations, DNA methylation, and miRNAs.

3.3. Phosphorylation of CSPP1 at specific sites may play a role in tumorigenesis, especially at Ser424

With datasets available in BRCA, GBM, HNSC, KIRC, LIHC, LUAD, OV, PAAD, and UCEC, CSPP1 protein expression was significantly increased in LIHC, PAAD, and UCEC compared with normal tissues; meanwhile, it was decreased in BRCA and HNSC (Fig. 3A; Fig. S4A).

Post-translational modification (PTM) is a key molecular mechanism associated with the activity of the protein [48]. A higher S31 phosphorylation level was observed in BRCA, GBM, LIHC, and LUAD; meanwhile, a lower level was observed in KIRC and PAAD. S424 phosphorylation was increased in BRCA, HNSC, KIRC, and LIHC. S847 phosphorylation was increased in HNSC but decreased in PAAD. Increased S866 phosphorylation was observed in HNSC and LIHC but decreased in KIRC, LUAD, and PAAD. S885 phosphorylation was increased in LIHC and decreased in KIRC. S931 phosphorylation was increased in LIHC and decreased in KIRC and LUAD (Fig. 3B, C; Fig. S4B). No threonine or tyrosine phosphorylation was identified in these cancer types with UALCAN database. Together, these findings suggested that phosphorylation of CSPP1 at specific sites may play a role in tumorigenesis, especially at Ser424.

3.4. CSPP1 correlates with clinical features and outcomes in multiple cancers

Thereafter, we investigated *CSPP1* expression at different pathologic stages, histologic grades, and molecular subtypes. *CSPP1* overexpression significantly correlated with advanced pathologic stage in READ, ACC, and KICH, and advanced histologic grade in HNSC and LIHC; however, high *CSPP1* expression correlated with low histologic grade in KIRC (Fig. 4A-D). In addition, *CSPP1* expression significantly differed with respect to molecular subtypes in BRCA, COAD, ESCA, LGG, LIHC, READ, LUSC, and UCEC (Fig. 4E, F). However, no association was observed in other cancers (Fig. S5).

To monitor the clinical outcomes of *CSPP1* differential expression, a Cox regression analysis was performed with respect to patients' prognoses. Results indicated that in *CSPP1*-upregulated cancers, *CSPP1* overexpression was associated with poor OS, DSS, and PFI in LGG and LIHC. In *CSPP1*-downregulated cancers, decreased *CSPP1* expression was associated with favorable OS, DSS, and PFI in ACC (Fig. 4G; Fig. S6). Overall, excessive *CSPP1* expression is unfavorable in several cancer types, especially LGG, LIHC, and ACC.

To further evaluate whether *CSPP1* was an independent risk factor for prognosis, we used LGG as an example ($p < 0.001$ for OS, DSS, and PFI). The baseline datasheet showed that *CSPP1* was significantly correlated with the WHO grade, IDH status, 1p/19q codeletion, and histological type (Table S4). Univariate Cox regression analyses further indicated that *CSPP1* correlated with poor prognosis. Furthermore, multivariate Cox regression analyses confirmed that *CSPP1* overexpressed as an independent factor associated with OS, DSS, and PFI (Fig. 4H, I; Fig. S7A, B, E, F). Based on the multivariate Cox regression analyses, nomogram prediction models were established (Fig. 4J; Fig. S7C, G). We performed calibration analysis on the nomograms to verify the validity of the predictive models. The C-indexes of OS, DSS, and PFI indicate median accuracy (Fig. 4K; Fig. S7D, H). These results confirmed *CSPP1* as an independent risk factor for LGG survival.

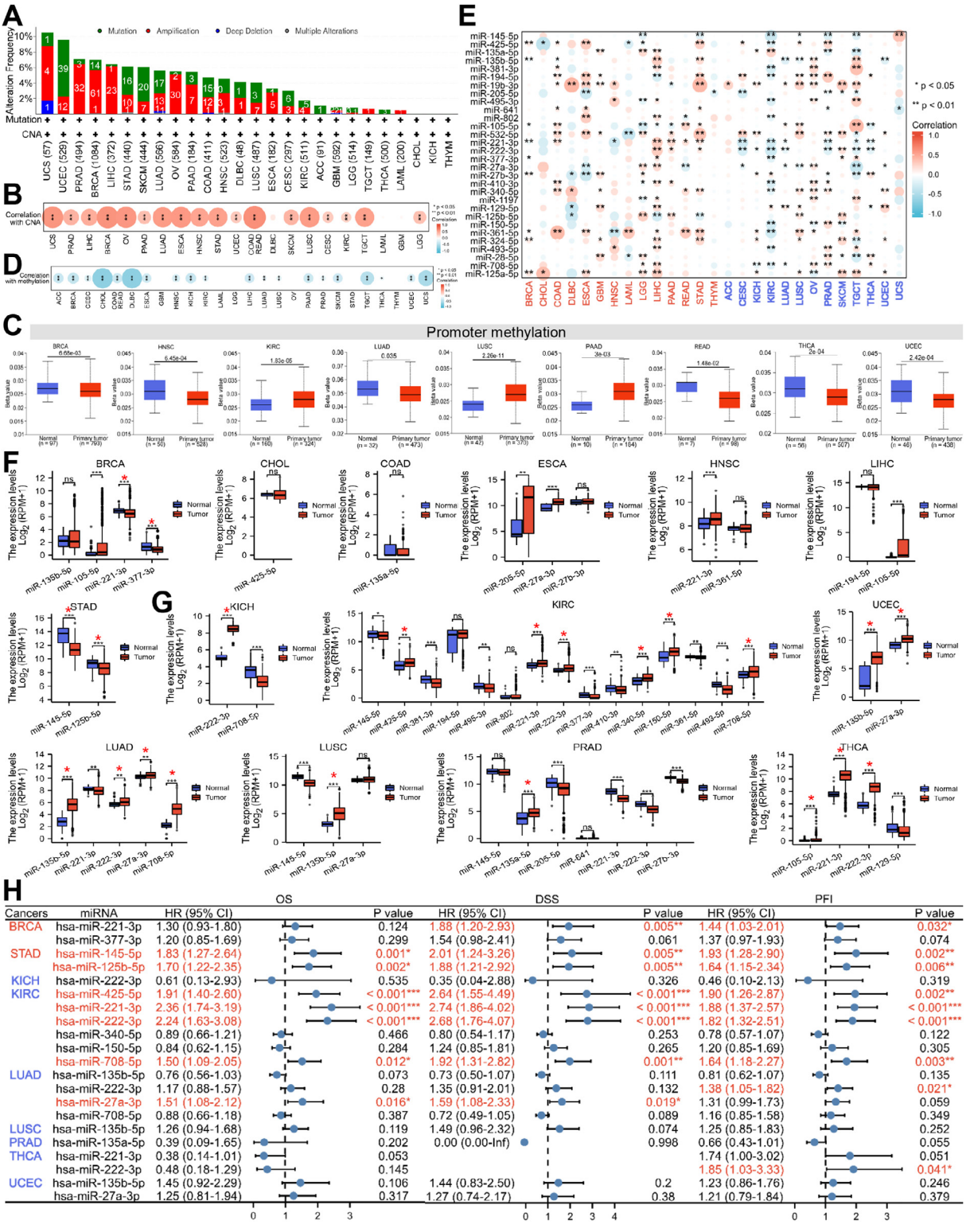

Cancers	miRNA	OS HR (95% CI)	OS P value	DSS HR (95% CI)	DSS P value	PFI HR (95% CI)	PFI P value
BRCA	hsa-miR-221-3p	1.30 (0.93-1.80)	0.124	1.88 (1.20-2.93)	0.005**	1.44 (1.03-2.01)	0.032*
	hsa-miR-377-3p	1.20 (0.85-1.69)	0.299	1.54 (0.98-2.41)	0.061	1.37 (0.97-1.93)	0.074
STAD	hsa-miR-145-5p	1.83 (1.27-2.64)	0.001*	2.01 (1.24-3.26)	0.005**	1.93 (1.28-2.90)	0.002**
	hsa-miR-125b-5p	1.70 (1.22-2.35)	0.002*	1.88 (1.21-2.92)	0.005**	1.64 (1.15-2.34)	0.006**
KICH	hsa-miR-222-3p	0.61 (0.13-2.93)	0.535	0.35 (0.04-2.88)	0.326	0.46 (0.10-2.13)	0.319
KIRC	hsa-miR-425-5p	1.91 (1.40-2.60)	< 0.001***	2.64 (1.55-4.49)	< 0.001***	1.90 (1.26-2.87)	0.002**
	hsa-miR-221-3p	2.36 (1.74-3.19)	< 0.001***	2.74 (1.86-4.02)	< 0.001***	1.88 (1.37-2.57)	< 0.001***
	hsa-miR-222-3p	2.24 (1.63-3.08)	< 0.001***	2.68 (1.76-4.07)	< 0.001***	1.82 (1.32-2.51)	< 0.001***
	hsa-miR-340-5p	0.89 (0.66-1.21)	0.466	0.80 (0.54-1.17)	0.253	0.78 (0.57-1.07)	0.122
	hsa-miR-150-5p	0.84 (0.62-1.15)	0.284	1.24 (0.85-1.81)	0.265	1.20 (0.85-1.69)	0.305
	hsa-miR-708-5p	1.50 (1.09-2.05)	0.012*	1.92 (1.31-2.82)	0.001**	1.64 (1.18-2.27)	0.003**
LUAD	hsa-miR-135b-5p	0.76 (0.56-1.03)	0.073	0.73 (0.50-1.07)	0.111	0.81 (0.62-1.07)	0.135
	hsa-miR-222-3p	1.17 (0.88-1.57)	0.28	1.35 (0.91-2.01)	0.132	1.38 (1.05-1.82)	0.021*
	hsa-miR-27a-3p	1.51 (1.08-2.12)	0.016*	1.59 (1.08-2.33)	0.019*	1.31 (0.99-1.73)	0.059
	hsa-miR-708-5p	0.88 (0.66-1.18)	0.387	0.72 (0.49-1.05)	0.089	1.16 (0.85-1.58)	0.349
LUSC	hsa-miR-135b-5p	1.26 (0.94-1.68)	0.119	1.49 (0.96-2.32)	0.074	1.25 (0.85-1.83)	0.252
PRAD	hsa-miR-135a-5p	0.39 (0.09-1.65)	0.202	0.00 (0.00-Inf)	0.998	0.66 (0.43-1.01)	0.055
THCA	hsa-miR-221-3p	0.38 (0.14-1.01)	0.053			1.74 (1.00-3.02)	0.051
	hsa-miR-222-3p	0.48 (0.18-1.29)	0.145			1.85 (1.03-3.33)	0.041*
UCEC	hsa-miR-135b-5p	1.45 (0.92-2.29)	0.106	1.44 (0.83-2.50)	0.2	1.23 (0.86-1.76)	0.246
	hsa-miR-27a-3p	1.25 (0.81-1.94)	0.317	1.27 (0.74-2.17)	0.38	1.21 (0.79-1.84)	0.379

Fig. 2. Multi-dimensional mechanisms involving genetic alterations, DNA methylation, and miRNAs underly *CSPP1* dysregulation. (A) Histogram of genetic alteration frequency of *CSPP1* from cBioPortal portal. (B) A heatmap of correlations between *CSPP1* and CNAs. Dot size together with transition color represented the degree of correlation. The larger the dot, the stronger the correlation. Red and blue represented positive and negative correlations, respectively. * $p < 0.05$, ** $p < 0.01$. (C) Histograms of *CSPP1* promoter methylation in normal and primary tumors with significant differences from UALCAN portal. $0.7 \geq$ Beta value > 0.5 was considered hyper-methylation, $0.3 \geq$ Beta value > 0.25 was hypo-methylation. (D) A heatmap of correlations between *CSPP1* and DNA methylation from cBioPortal portal. (E) A heatmap of correlation between *CSPP1* and predicted miRNAs from ENCORI portal. Red and blue words indicated upregulated and downregulated cancers, respectively. (F, G) Differential expression of negatively associated miRNAs from TCGA database. Red stars represent negatively correlated miRNAs of *CSPP1*. (H) A forest plot of the correlations between *CSPP1*-negatively associated miRNAs expression and survival probability, including OS, DSS, and PFI. * $p < 0.05$, ** $p < 0.01$, *** $p < 0.001$. (For interpretation of the references to color in this figure legend, the reader is referred to the web version of this article.)

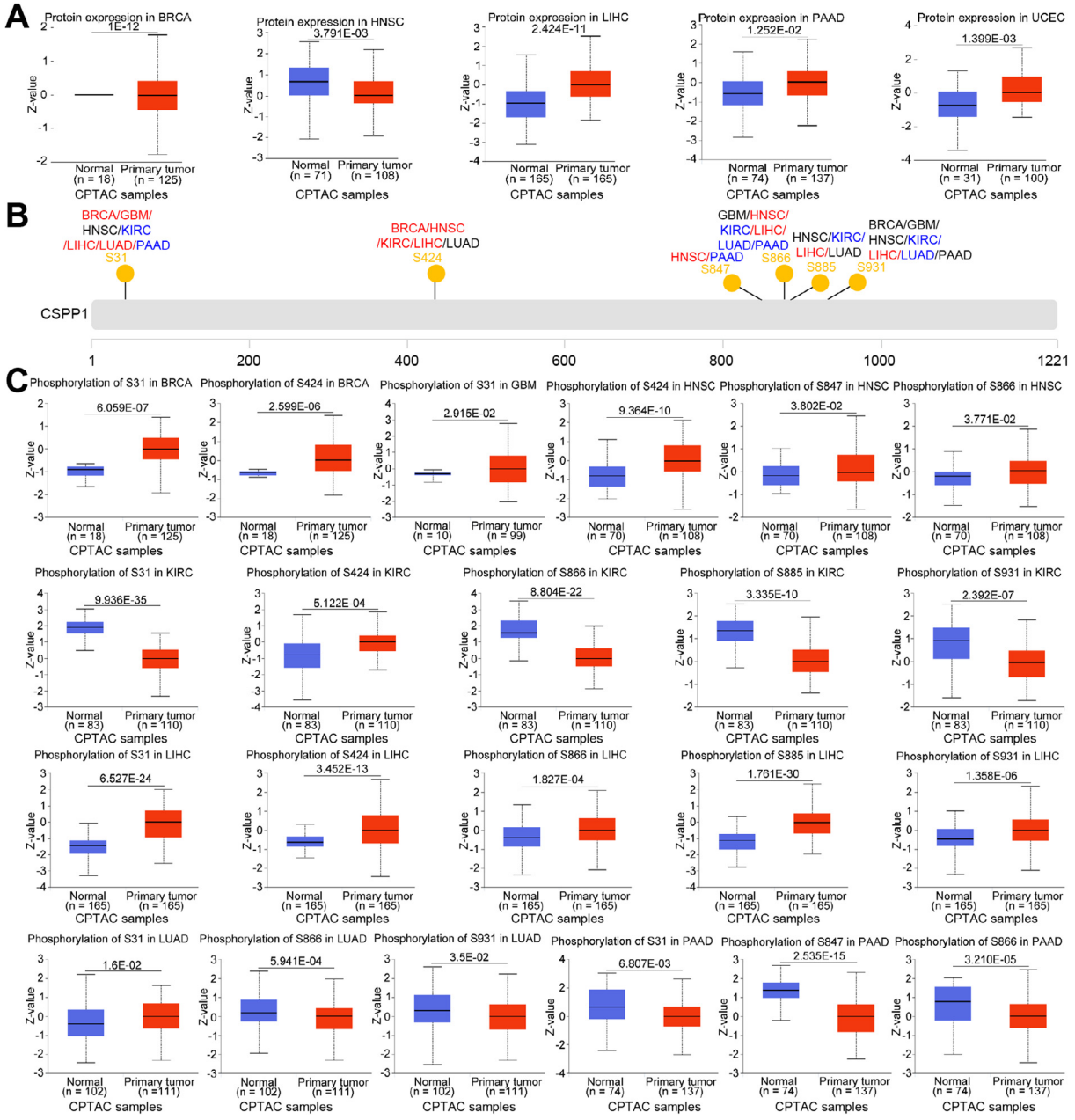

Fig. 3. Phosphorylation of CSPP1 at specific sites may play a role in tumorigenesis, especially at Ser424. (A) Histograms of CSPP1 expression in nine types of the normal and primary tumors with significant differences using CPTAC samples from UALCAN portal. (B) The schematic diagram of CSPP1 phosphorylation sites. Red and blue words indicated high and low protein expression, respectively. (C) Histograms of the phosphorylation site of CSPP1 in normal and primary tumors with significant differences. $p < 0.05$ was considered statistically significant. (For interpretation of the references to color in this figure legend, the reader is referred to the web version of this article.)

3.5. Functional enrichment indicates CSPP1 is potentially associated with ferroptosis and TME in LGG

Based on its unfavorable prognosis, LGG patients were divided into high and low *CSPP1* expression groups, and mRNA expression patterns were compared. A total of 14 upregulated and 67 downregulated genes were identified (Fig. 5A). Correlations between *CSPP1* and the top 20 DEGs were visualized by a heatmap (Fig. 5B; Table S5).

GO and GSEA analyses were performed to investigate the functional mechanisms of *CSPP1*. *CSPP1*-related DEGs were enriched in (i) CCs: presynapse, transport vesicle, and synaptic membrane; (ii) MFs: passive transmembrane transporter activity, channel activity, and substrate-specific channel activity; and (iii) BPs: signal release, vesicle-mediated transport in synapse, and regulation of transporter activity (Fig. 5C; Table S6). GSEA was also used to identify *CSPP1*-associated pathways. The results suggested that, in hallmark gene sets, *CSPP1*-related DEGs were positively related to cell cycle-related pathways (E2F targets, G2/M checkpoint, and mitotic spindle), cancer-related pathways (Notch signaling and TGF-β signaling), EMT, and inflammatory response; meanwhile, they were negatively related to KRAS signaling DN, ferroptosis-related metabolic pathways (fatty acid metabolism, cholesterol homeostasis, and oxidative phosphorylation). For GO and KEGG gene sets, *CSPP1*-related DEGs were positively associated with cell cycle-related pathways (cell cycle checkpoint, chromosome segregation, and microtubule cytoskeleton organization involved in mitosis), cancer-related pathways (Notch signaling pathway, TGF-β signaling pathway, and pathways in cancer), stromal-related pathway (ECM structural constituent, extracellular structure organization,

ECM receptor interaction, and focal adhesion), and immune-related pathways (B cell-mediated immunity, adaptive immune response, positive regulation of T cell proliferation, T cell activation involved in immune response, complement and coagulation cascades, intestinal immune network for IgA production, cytosolic DNA sensing pathway, and toll-like receptor signaling pathway); meanwhile, they were negatively associated with ferroptosis-related metabolic pathways (steroid metabolic process, steroid biosynthetic process, response to metal ion, terpenoid backbone biosynthesis, and oxidative phosphorylation) (Fig. 5D; Table S7). These findings implied that *CSPP1* may be involved in ferroptosis and TME.

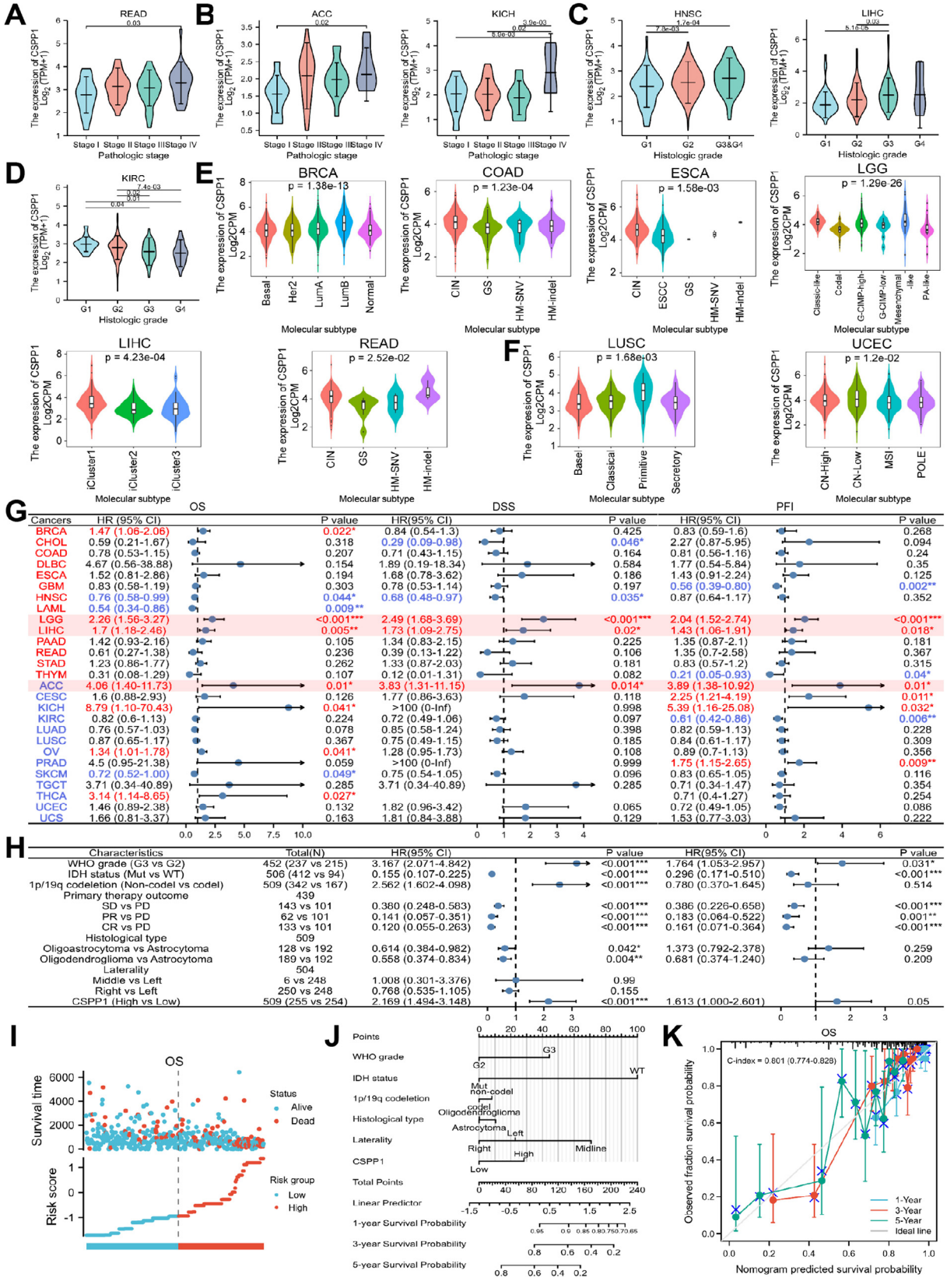

3.6. CSPP1 dysregulates ferroptosis in LGG and other cancer types

TP53 is the most commonly mutated gene associated with cancers and its mutations have been reported to be closely associated with ferroptosis [49–55]. To verify the correlation between *TP53* mutation and *CSPP1* expression, somatic mutation analysis was performed according to *CSPP1* expression in LGG. From the oncoplot, higher frequencies of *TP53* and *ATRX* mutations and lower frequencies of *CIC*, *FUBP1*, *NOTCH1*, *IDH2*, and *ZBTB20* mutations were observed in the high *CSPP1* expression group (Fig. 6A, B). However, no association between *ATRX*, *CIC*, *FUBP1*, *NOTCH1*, *IDH2*, and *ZBTB20* mutations and ferroptosis has been reported.

To further confirm the correlation between *CSPP1* and ferroptosis, 30 ferroptosis-associated genes (FAGs) were extracted from KEGG, including 18 ferroptosis-driver genes (FDGs) of *ACSL1*, *ACSL4*, *ACSL6*, *ALOX15*, *ATG5*, *ATG7*, *FTL*, *LPCAT3*, *MAP1LC3A*, *MAP1LC3B*, *NCOA4*, *SAT1*, *SLC39A14*, *TF*, *TFRC*, *TP53*, *VDAC2*, *VDAC3* and 12 ferroptosis-suppressor genes (FSGs) of *ACSL3*, *FTH1*, *FTMT*, *GCLC*, *GCLM*, *GPX4*, *GSS*, *HMOX1*, *PCBP1*, *SLC3A2*, *SLC7A11*, *SLC40A1* [56–59]. We found that *CSPP1* positively correlated with most FAGs, but negatively correlated with two FDGs of *FTL*, *MAP1LC3A*, and three FSGs of *FTH1*, *GPX4*, and *HMOX1* (Fig. 6C; Table S8).

Next, the overall scores of driver genes and suppressor genes were calculated by the ssGSEA algorithm, and the ferroptosis score obtained from driver score minus suppressor score was used to evaluate whether the function of *CSPP1* was to activated or inhibited ferroptosis in cancers. The gene set and its corresponding algorithm have been proved to be able to predict ferroptosis status [56–59]. In *CSPP1*-upregulated cancers, *CSPP1* positively correlated with ferroptosis score in LAML; meanwhile, negative correlations were observed in BRCA, GBM, LGG, LIHC, and THYM. In *CSPP1*-downregulated cancers, positive correlations were exhibited in ACC and LUAD, while negative correlations existed in KIRC, OV, and PRAD (Fig. 6D; Table S8). These tumor samples were further divided into high and low *CSPP1* expression groups, and the ferroptosis score was further compared between the two groups. From the histogram, as an antitumor mechanism, ferroptosis was overall inhibited in pan-cancer (ferroptosis score < 1), except for LAML. Lower scores represented lower ferroptosis levels in BRCA, COAD, GBM, LGG, LIHC, THYM, OV, and PRAD and higher scores represented higher ferroptosis levels in LAML and ACC were observed in the high *CSPP1* expression group (Fig. 6E; Table S8). Thus, our findings revealed that *CSPP1* dysregulates ferroptosis in LGG and other cancer types.

3.7. CSPP1-associated tumors are infiltrated in different TMEs, improving ICB therapeutic efficacy in specific cancers

Functional enrichment analysis also implied that *CSPP1* may regulate the TME by influencing the immune response and stromal response. Therefore, we performed a pan-cancer analysis of the correlation between *CSPP1* and these two components. We first focused on *CSPP1* and 24 types of immune cells using the ssGSEA algorithm. The results showed that *CSPP1* negatively correlated with most immune cells across cancers but positively correlated with T helper cells, central memory T (Tcm) cells, and T helper 2 (Th2) cells. Of note, Tcm cells are also immunosuppressive cells. Next, stromal cell infiltration was assessed using the XCELL algorithm from the TIMER2 portal, mainly including CAF cells and endothelial cells [60]. There was a positive correlation between *CSPP1* and CAFs in HNSC, LGG, LIHC, THYM, KICH, SKCM, and THCA, whereas an inverse correlation was observed in STAD, KIRC, LUSC, and TGCT. Moreover, *CSPP1* was negatively correlated with endothelial cells in BRCA, DLBC, LGG, LIHC, STAD, THYM, PRAD, TGCT, and UCEC, whereas a positive correlation was noted in OV. Thereafter, we comprehensively calculated the TME score using the ESTIMATE package. *CSPP1* was negatively associated with the stromal score, immune score, and ESTIMATE score in most cancers, while positively associated with these scores in LGG (Fig. 7A; Table S9). To sum up, *CSPP1* comprehensively regulates the TME from both immune cell infiltration and stromal cell infiltration.

To further study the regulatory mechanism of *CSPP1*-related tumor infiltration, correlations between *CSPP1* and three types of immunomodulators were investigated with TCGA datasets [61]. *CSPP1* negatively correlated with MHCs and positively with immune stimulators and immune inhibitors in most cancers (Fig. 7B; Table S9). Among immune inhibitors, *CD274* (PD-L1), *CTLA4, HAVCR2, LAG3, PDCD1* (PD1), *PDCD1LG2* (PD-L2), *TIGIT*, and *SIGLEC15* are known immune checkpoints responsible for tumor immune escape. Combined with these immune checkpoint results and subsequent analysis using the TIMER2 portal, it was further confirmed that *CSPP1* was positively correlated with immune checkpoints in BRCA, DLBC, ESCA, HNSC, LGG, LIHC, PAAD, READ, KICH, and KIRC, and negatively correlated with them in COAD, LAML, CESC, THCA, and UCEC (Fig. 7B, C; Table S9).

TMB and MSI are two emerging biomarkers associated with immunotherapy response. Tumor cells with high TMB or MSI scores have strong antigenicity and more neoantigens, thus promoting immune cell infiltration. Results showed that *CSPP1* positively correlated with TMB in LGG, STAD, and PRAD, but inversely correlated with it in COAD, LIHC, THCA, and UCEC. The correlation between *CSPP1* and MSI was then investigated. LGG, READ, STAD, LUAD, and LUSC showed positive correlations, whereas DLBC presented a negative correlation (Fig. 7D; Table S9).

Tumor immunotherapy is a treatment that controls and eliminates tumors by reactivating and maintaining the tumor-immune cycle and restoring the normal antitumor immune response, including ICB and cell therapy. The effectiveness of ICB therapy depends not only on immune cell infiltration but also on immune checkpoints, TMB, and MSI. The close correlations between *CSPP1* and immune checkpoints, TMB, and MSI implied that these *CSPP1*-associated tumor patients may respond well to immunotherapy. Therefore, the TIDE algorithm was used to predict the therapeutic effect of ICB from TCGA database. Results revealed that in *CSPP1*-upregulated cancers, the high *CSPP1* expression group exhibited a lower TIDE score, including BRCA, DLBC, LGG, and STAD; meanwhile, the low *CSPP1* expression group exhibited a lower TIDE score in LIHC (Fig. 7E; Fig. S8A). In *CSPP1*-downregulated cancers, the high *CSPP1* expression group exhibited a lower TIDE score, including CESC, KIRC, LUSC, PRAD, SKCM, TGCT, THCA, and UCES (Fig. 7F; Fig. S8B). It is suggested that these patients with low TIDE scores may benefit from ICB therapy.

Fig. 4. *CSPP1* correlates with clinical features and outcomes in multiple cancers. (A-D) Violin plots of correlation between *CSPP1* expression and pathologic stage (A, B) and histologic grade (C, D) from TCGA database with significant differences using Kruskal-Wallis test. (E, F) Violin plots of correlation between *CSPP1* expression and molecular subtype with significant differences from TISIDB portal. $p < 0.05$ was considered as a statistical difference between the two groups. (G) A forest plot of the correlations between *CSPP1* expression and survival probability, including OS, DSS, and PFI. (H) A forest plot of univariate and multivariate Cox regression analyses with OS in LGG from TCGA database. *p* represented the overall difference. * $p < 0.05$, ** $p < 0.01$, *** $p < 0.001$. (I) Identification of *CSPP1* as an independent risk factor in LGG. The upper portion scatters plot was survival time and survival status according to *CSPP1* expression, and the middle portion scatters plot was risk score. (J) Construction of a prognostic nomogram in LGG. (K) Nomogram calibration analysis with prognostic data in LGG. C-index > 0.9 indicated highly accuracy, 0.9 ≥ C-index > 0.7 was median, and 0.7 ≥ C-index > 0.5 was low.

4. Discussion

Cancer is the leading cause of morbidity and mortality worldwide. *CSPP1* is a centrosome and microtubule-binding protein that

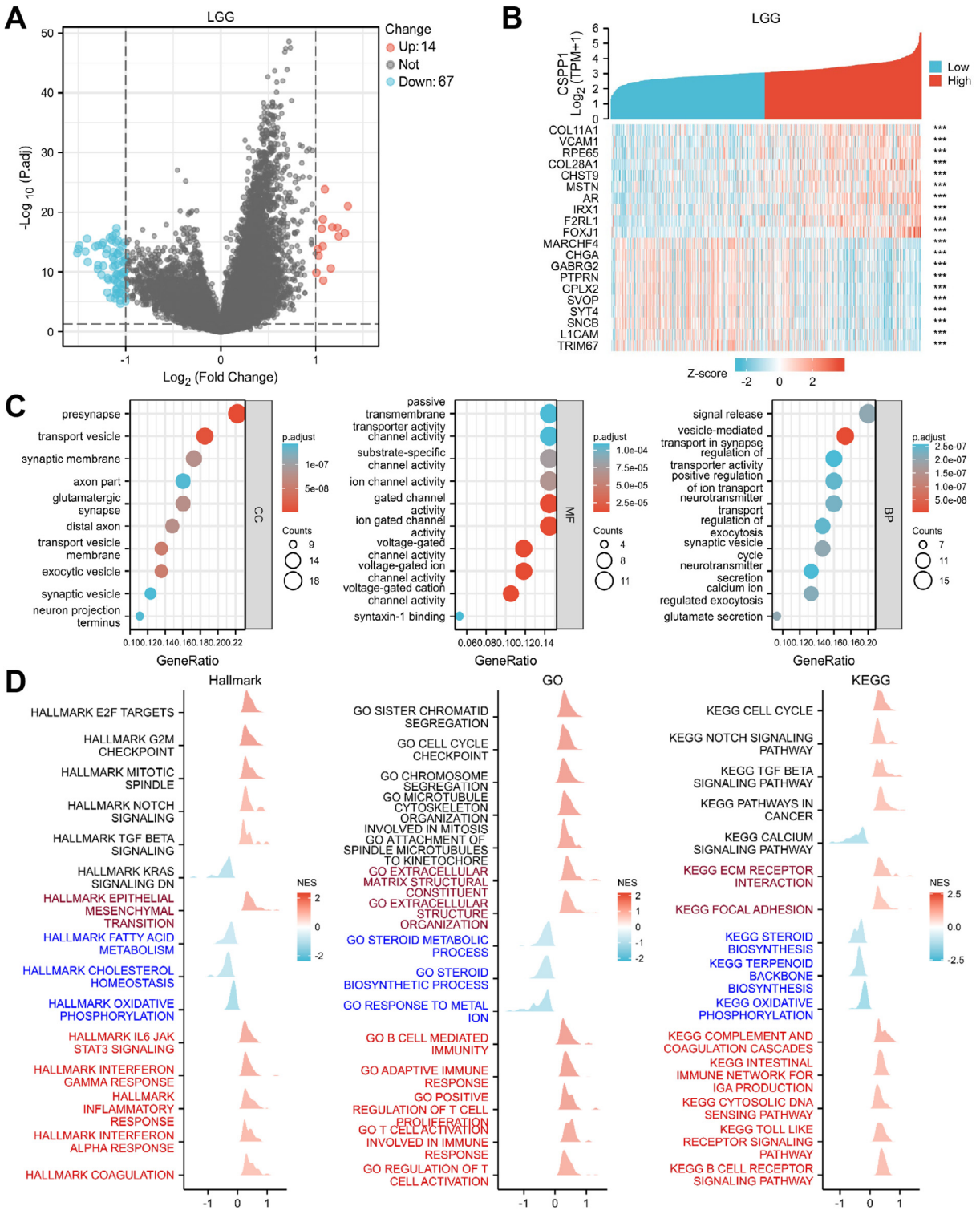

Fig. 5. Functional enrichment indicates that *CSPP1* is potentially associated with ferroptosis and TME in LGG. (A) A volcano plot of *CSPP1*-related DEGs in LGG. Red and blue points indicated upregulated and downregulated genes, respectively. (B) A heatmap of correlation between *CSPP1* and the top 20 DEGs. *** $p < 0.001$. (C) Bubble plots of GO enrichment. The X-axis represents the ratio of these DEGs, and the Y-axis represents the categories of DEGs. (D) Ridge plots of GSEA enrichment. $p < 0.05$ was considered the meaningful pathway. Red and blue indicated immune-related pathways and ferroptosis-related metabolic pathways, respectively. (For interpretation of the references to color in this figure legend, the reader is referred to the web version of this article.)

plays a role in cell cycle-dependent cytoskeleton organization and cilia formation. Although there is increasing evidence that *CSPP1* may play a role in tumorigenesis, its specific role across different cancers remains unclear. This study systematically analyzed *CSPP1* expression and demonstrated that its aberrant expression in 27 cancer types is driven by multi-dimensional mechanisms. *CSPP1* correlates with clinical features and serves as a potential diagnostic and prognostic biomarker as well as the target for ferroptosis-based drug therapy and immunotherapy.

To explore how *CSPP1* influences the progress and prognosis of cancer, its effects on ferroptosis and TME were studied. Function enrichment demonstrated that *CSPP1* was involved in ferroptosis-

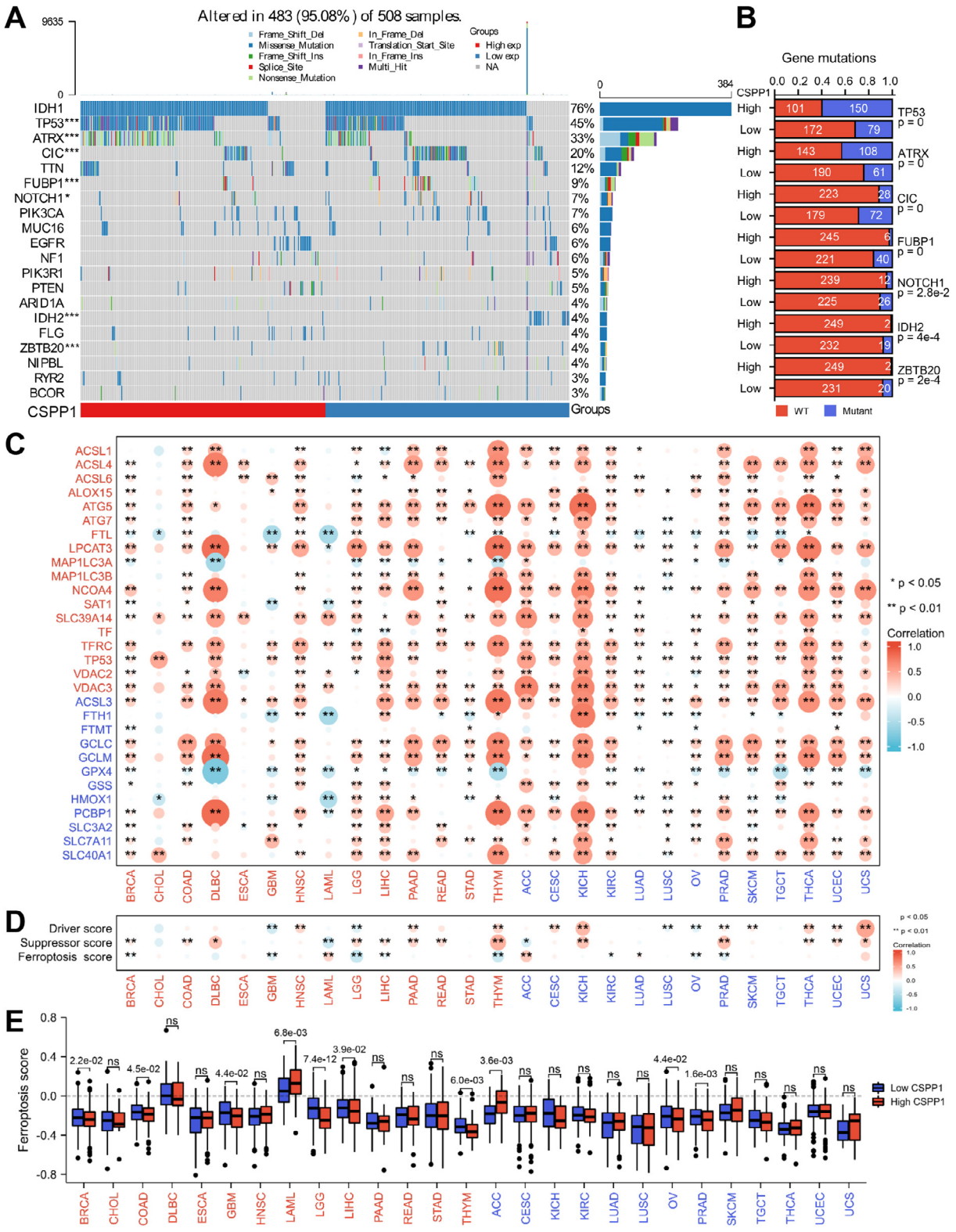

Fig. 6. *CSPP1* dysregulates ferroptosis in LGG and other cancer types. (A) Oncoplot of somatic mutant landscape in high and low *CSPP1* expression groups in LGG. * $p < 0.05$, ** $p < 0.01$, *** $p < 0.001$. (B) Histograms of gene mutants comparison in high and low *CSPP1* expression groups by chisq.test with significant differences. (C, D) Heatmaps of correlation between *CSPP1* and FAGs and ferroptosis-associated scores. Dot size together with transition color represented the degree of correlation. The larger the dot, the stronger the correlation. Red and blue dots represented positive and negative correlations, respectively. * $p < 0.05$, ** $p < 0.01$. (E) Histograms of ferroptosis scores between high and low *CSPP1* expression groups from TCGA database. $p < 0.05$ was considered statistically significant. (For interpretation of the references to color in this figure legend, the reader is referred to the web version of this article.)

related metabolic pathways. Mutation analyses further indicated that *CSPP1* was closely associated with *TP53* mutation, which has been reported to be associated with cancer and ferroptosis, thus speculating that *CSPP1* might correlate with ferroptosis. At present, studies on ferroptosis-associated gene mutations are mainly limited to the oncogenes and tumor suppressor genes, including onco-

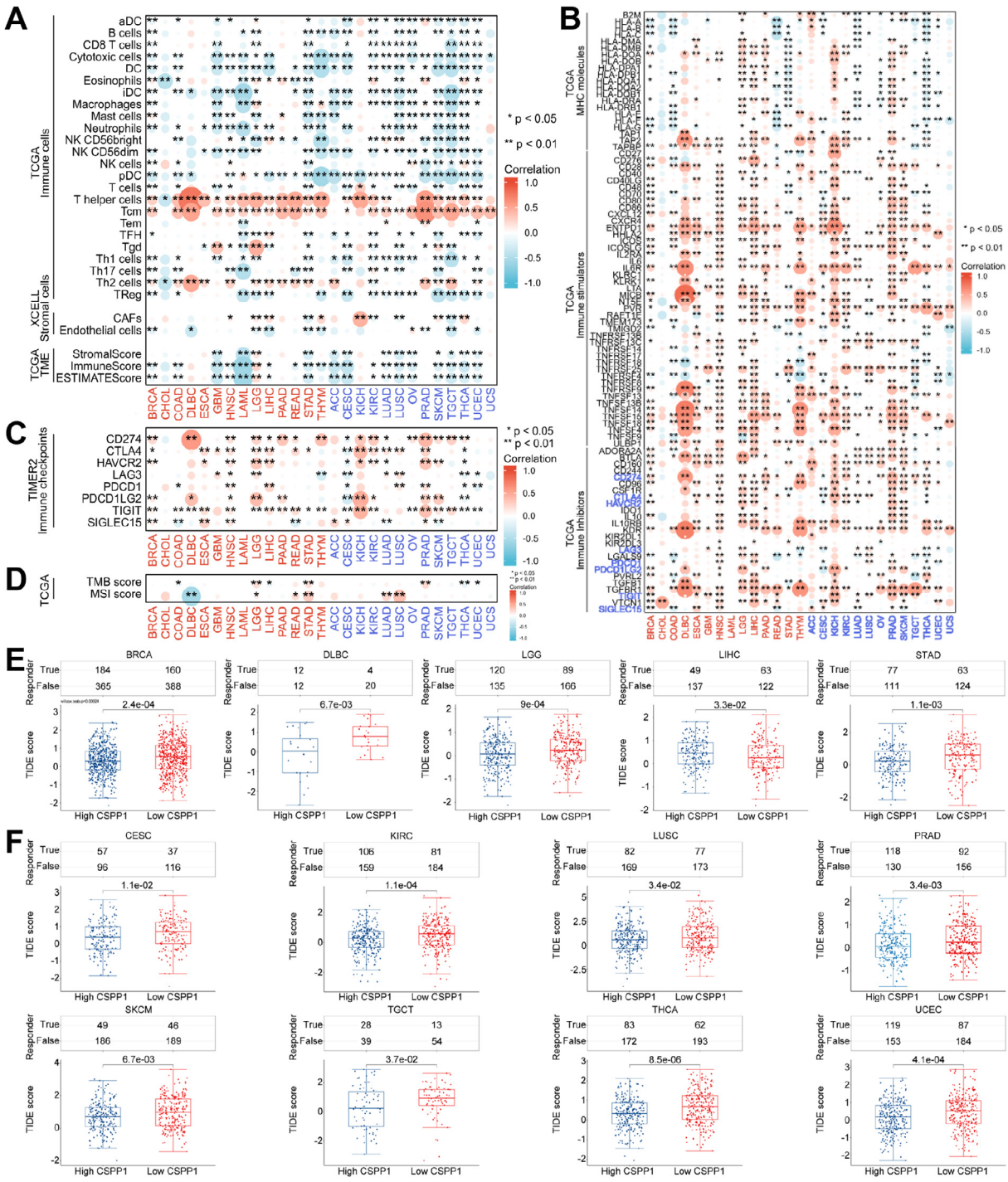

Fig. 7. *CSPP1*-associated tumors are infiltrated in different TMEs, improving ICB therapeutic efficacy in specific cancers. (A) A heatmap of correlations between *CSPP1* and 24 types of immune cells from TCGA database, CAFs and endothelial cells from TIMER2 portal using XCELL algorithm, and TME scores from TCGA database using the ssGSEA algorithm. (B) A heatmap of correlations between *CSPP1* and immunomodulators, including MHC molecules, immune stimulator genes, and immune inhibitor genes from TCGA database. (C) A heatmap of correlations between *CSPP1* and immune checkpoints from the TIMER2 portal. (D) A heatmap of correlations between *CSPP1* and TMB score, MSI score from TCGA database. Dot size together with transition color represented the degree of correlation. The larger the dot, the stronger the correlation. Red and blue dots represented positive and negative correlation, respectively. * $p < 0.05$, ** $p < 0.01$. (E, F) Histograms of *CSPP1*-associated ICB therapeutic effect between high and low *CSPP1* expression groups from TCGA database by TIDE algorithm with a significant difference. A low score indicated good efficacy. $p < 0.05$ was considered statistically significant. (For interpretation of the references to color in this figure legend, the reader is referred to the web version of this article.)

genes of *PIK3CA*, *KRAS*, *NEDD4*, *VDAC2/3*, *DJ1*, *PDK4*, and tumor suppressor genes of *TP53*, *BAP1*, *KEAP1, ARF*. Activating mutations in oncogenes and inactivating mutations in tumor suppressor genes regulate the expression of FAGs, and generally tend to inhibit ferroptosis and promote tumor progression. However, mutations in tumor suppressors of the *E-cadherin-NF2-Hippo* axis, *VHL*, and oncogenes of *EGFR* and *IDH1* render cancer cells vulnerable to ferroptosis in one or more cancer types [62,63]. Our correlation analyses between *CSPP1* and FAGs and ferroptosis-associated scores further confirmed that *CSPP1* was indeed involved in the regulation of ferroptosis in pan-cancer. Combined with the prognostic data, we believed that in *CSPP1*-upregulated cancers, *CSPP1* overexpres-

sion inhibited ferroptosis, including BRCA, GBM, LGG, LIHC, and THYM, thus promoting tumor cell growth and leading to poor prognoses in BRCA, LGG, and LIHC. Meanwhile, its overexpression promoted ferroptosis in LAML and led to cancer with a good prognosis. These results were consistent with the progression and prognosis results of *CSPP1*. However, there were some exceptions. For example, patients with lower expression of *CSPP1* showed lower ferroptosis level but better prognosis in ACC, and higher ferroptosis levels but still led to cancer in OV and PRAD. Thus, there should be other mechanisms influencing the progression and prognosis of these cancers. For *CSPP1*-associated tumors with suppressed ferroptosis, drug-induced ferroptosis through the *CSPP1*-FDGs or *CSPP1*-FSGs axis may inhibit tumor progression and thus improve prognosis. Therefore, the possibility of drug therapy for *CSPP1*-associated tumor patients by regulating ferroptosis is proposed.

In addition to regulating ferroptosis, *CSPP1* may have a regulatory role in the TME by affecting EMT, stromal-related pathways, and immune-related pathways. In recent years, an increasing number of studies have linked microtubule-associated genes to immune infiltration. High expression of Targeting Protein for Xenopus kinesin-like protein 2 (*TPX2*) and Tubulin alpha-1C chain (*TUBA1C*) increases immune cell infiltration in LIHC, LUAD, and LGG, respectively, and is associated with poor prognosis [64–66]. A high level of microtubule-associated protein *Tau* is inversely correlated with the vascular and immune contents, delaying tumor growth in gliomas [67]. Increased expression of microtubule interacting and trafficking domain containing 1 (*MITD1*) indicates a poor prognosis with decreased NK cell infiltration in LIHC and increased CD8+ T cells infiltration in KIRC [68,69]. Spindle and kinetochore-associated protein (*Ska*) complex negatively and positively correlate with immune cell infiltration in BRCA and LIHC, respectively [70,71]. In our study, *CSPP1* comprehensively regulated the TME from both immune cell infiltration and stromal cell infiltration. *CSPP1* was negatively correlated with immune scores, stromal scores, and TME scores for most cancers. Moreover, it was also negatively correlated with MHCs and positively associated with immune stimulators and immune inhibitors, including immune checkpoints. *CSPP1* expression also significantly correlated with TMB and MSI in specific cancers. ICB therapy prediction confirmed that these cancer patients could benefit from ICB therapy, thus promoting a favorable prognosis. Specifically, in *CSPP1*-upregulated cancers, low TME scores and high levels of immune checkpoints expression indicated immune infiltration was greatly suppressed, leading to tumor growth and poor prognosis. Therefore, ICB therapy promoting immune infiltration is effective for patients in the high *CSPP1* expression group of BRCA, DLBC, LGG, and STAD, but more effective for patients in the low *CSPP1* expression group of LIHC. In *CSPP1*-downregulated cancer, low *CSPP1* expression had higher levels of immune cell infiltration and lower levels of immune checkpoints expression, thus these cancers themselves were in a favorable prognostic immune microenvironment, and ICB therapy may be more effective for the early treatment of these patients, including CESC, KIRC, LUSC, PRAD, SKCM, TGCT, THCA, and UCEC.

However, several limitations still remain. At present, our study on the regulation of *CSPP1* on ferroptosis and TME, as well as the subsequent potential drug treatment and ICB therapy are limited to bioinformatics, which provides a reference to basic experiments, but basic experiments are still necessary for follow-up research. In addition, the relatively small sample size is also one of the main reasons for data deviation. For example, as described above, the regulation of *CSPP1* expression involves multiple factors, which leads to the inconsistency between any individual factor and *CSPP1* expression, and the small sample size increases this inconsistency. In addition, the inconsistent expression between *CSPP1* mRNA and protein is the same case. Therefore, further basic experiments and more clinical samples are required to explore the direct functional mechanism of *CSPP1* affecting cancer progression and prognosis through ferroptosis and TME function.

5. Conclusion

In conclusion, our study is the first to demonstrate that *CSPP1* is a potential diagnostic and prognostic biomarker associated with ferroptosis and TME, providing a new target for ferroptosis-based drug therapy and immunotherapy in specific cancer types.

Author contributions

SZ contributed to the conception of the study. WW designed the study and wrote the manuscript. WW, JZ, YW, and YX had full access to all of the data in the study and take responsibility for the integrity of the data. WW, JZ, YW, and YX performed the statistical analyses. SZ obtained funding. All authors contributed to the article and approved the submitted version.

Funding information

This work was supported by the National Natural Science Foundation of China (81773242), Zhejiang Provincial Natural Science Foundation of China (LY19H160032), and Major Project of Hangzhou Science and Technology Bureau (20180417A01).

Declaration of Competing Interest

The authors declare that they have no known competing financial interests or personal relationships that could have appeared to influence the work reported in this paper.

Acknowledgements

We thank the members of our research center for inspiring discussion.

Appendix A. Supplementary data

Supplementary data to this article can be found online at https://doi.org/10.1016/j.csbj.2022.06.046.

References

[1] Hanahan D. Hallmarks of cancer: new dimensions. Cancer Discov 2022;12:31–46.
[2] Dixon SJ, Stockwell BR. The hallmarks of ferroptosis. Ann Rev Cancer Biol 2019;3:35–54.
[3] Moujalled D, Strasser A, Liddell JR. Molecular mechanisms of cell death in neurological diseases. Cell Death Differ 2021;28:2029–44.
[4] Stockwell BR, Friedmann Angeli JP, Bayir H, Bush AI, Conrad M, et al. Ferroptosis: A regulated cell death nexus linking metabolism, redox biology, and disease. Cell 2017;171:273–85.
[5] Wang W, Green M, Choi JE, Gijon M, Kennedy PD, et al. CD8(+) T cells regulate tumour ferroptosis during cancer immunotherapy. Nature 2019;569:270–4.
[6] Sun LL, Linghu DL, Hung MC. Ferroptosis: a promising target for cancer immunotherapy. Am J Cancer Res 2021;11:5856–63.
[7] Turley SJ, Cremasco V, Astarita JL. Immunological hallmarks of stromal cells in the tumour microenvironment. Nat Rev Immunol 2015;15:669–82.
[8] Bruni D, Angell HK, Galon J. The immune contexture and Immunoscore in cancer prognosis and therapeutic efficacy. Nat Rev Cancer 2020;20:662–80.
[9] Zhou J, Kryczek I, Li S, Li X, Aguilar A, et al. The ubiquitin ligase MDM2 sustains STAT5 stability to control T cell-mediated antitumor immunity. Nat Immunol 2021;22:460–70.
[10] Zou W. Immune regulation in the tumor microenvironment and its relevance in cancer therapy. Cell Mol Immunol 2022;19:1–2.
[11] Patzke S, Hauge H, Sioud M, Finne EF, Sivertsen EA, et al. Identification of a novel centrosome/microtubule-associated coiled-coil protein involved in cell-cycle progression and spindle organization. Oncogene 2005;24:1159–73.

[12] Patzke S, Stokke T, Aasheim HC. CSPP and CSPP-L associate with centrosomes and microtubules and differently affect microtubule organization. J Cell Physiol 2006;209:199–210.
[13] Asiedu M, Wu D, Matsumura F, Wei Q. Centrosome/spindle pole-associated protein regulates cytokinesis via promoting the recruitment of MyoGEF to the central spindle. Mol Biol Cell 2009;20:1428–40.
[14] Zhu L, Wang Z, Wang W, Wang C, Hua S, et al. Mitotic protein CSPP1 interacts with CENP-H protein to coordinate accurate chromosome oscillation in mitosis. J Biol Chem 2015;290:27053–66.
[15] Frikstad KM, Molinari E, Thoresen M, Ramsbottom SA, Hughes F, et al. A CEP104-CSPP1 complex is required for formation of primary cilia competent in hedgehog signaling. Cell Rep 2019;28. 1907–22 e6.
[16] Patzke S, Redick S, Warsame A, Murga-Zamalloa CA, Khanna H, et al. CSPP is a ciliary protein interacting with Nephrocystin 8 and required for cilia formation. Mol Biol Cell 2010;21:2555–67.
[17] Shearer RF, Frikstad KM, McKenna J, McCloy RA, Deng N, et al. The E3 ubiquitin ligase UBR5 regulates centriolar satellite stability and primary cilia. Mol Biol Cell 2018;29:1542–54.
[18] Latour BL, Van De Weghe JC, Rusterholz TD, Letteboer SJ, Gomez A, et al. Dysfunction of the ciliary ARMC9/TOGARAM1 protein module causes Joubert syndrome. J Clin Invest 2020;130:4423–39.
[19] Ben-Omran T, Alsulaiman R, Kamel H, Shaheen R, Alkuraya FS. Intrafamilial clinical heterogeneity of CSPP1-related ciliopathy. Am J Med Genet A 2015;167A:2478–80.
[20] Tuz K, Bachmann-Gagescu R, O'Day DR, Hua K, Isabella CR, et al. Mutations in CSPP1 cause primary cilia abnormalities and Joubert syndrome with or without Jeune asphyxiating thoracic dystrophy. Am J Hum Genet 2014;94:62–72.
[21] Shaheen R, Shamseldin HE, Loucks CM, Seidahmed MZ, Ansari S, et al. Mutations in CSPP1, encoding a core centrosomal protein, cause a range of ciliopathy phenotypes in humans. Am J Hum Genet 2014;94:73–9.
[22] Akizu N, Silhavy JL, Rosti RO, Scott E, Fenstermaker AG, et al. Mutations in CSPP1 lead to classical Joubert syndrome. Am J Hum Genet 2014;94:80–6.
[23] Sternemalm J, Geimer S, Frikstad KA, Schink KO, Stokke T, et al. CSPP-L associates with the desmosome of polarized epithelial cells and is required for normal spheroid formation. PLoS ONE 2015;10:e0134789.
[24] Sternemalm J, Russnes HG, Zhao X, Risberg B, Nord S, et al. Nuclear CSPP1 expression defined subtypes of basal-like breast cancer. Br J Cancer 2014;111:326–38.
[25] Ribeiro IP, Marques F, Barroso L, Rodrigues J, Caramelo F, et al. Genomic profile of oral squamous cell carcinomas with an adjacent leukoplakia or with an erythroleukoplakia that evolved after the treatment of primary tumor: A report of two cases. Mol Med Rep 2017;16:6780–6.
[26] Liu J, Lichtenberg T, Hoadley KA, Poisson LM, Lazar AJ, et al. An integrated TCGA pan-cancer clinical data resource to drive high-quality survival outcome analytics. Cell 2018;173. 400-16 e11.
[27] Vivian J, Rao AA, Nothaft FA, Ketchum C, Armstrong J, et al. Toil enables reproducible, open source, big biomedical data analyses. Nat Biotechnol 2017;35:314–6.
[28] Chen F, Chandrashekar DS, Varambally S, Creighton CJ. Pan-cancer molecular subtypes revealed by mass-spectrometry-based proteomic characterization of more than 500 human cancers. Nat Commun 2019;10:5679.
[29] Chandrashekar DS, Bashel B, Balasubramanya SAH, Creighton CJ, Ponce-Rodriguez I, et al. UALCAN: A portal for facilitating tumor subgroup gene expression and survival analyses. Neoplasia 2017;19:649–58.
[30] Li JH, Liu S, Zhou H, Qu LH, Yang JH. starBase v2.0: decoding miRNA-ceRNA, miRNA-ncRNA and protein-RNA interaction networks from large-scale CLIP-Seq data. Nucleic Acids Res 2014;42:D92–7.
[31] Ru B, Wong CN, Tong Y, Zhong JY, Zhong SSW, et al. TISIDB: an integrated repository portal for tumor-immune system interactions. Bioinformatics 2019;35:4200–2.
[32] Love MI, Huber W, Anders S. Moderated estimation of fold change and dispersion for RNA-seq data with DESeq2. Genome Biol 2014;15:550.
[33] Yu G, Wang LG, Han Y, He QY. clusterProfiler: an R package for comparing biological themes among gene clusters. OMICS 2012;16:284–7.
[34] Mayakonda A, Lin DC, Assenov Y, Plass C, Koeffler HP. Maftools: efficient and comprehensive analysis of somatic variants in cancer. Genome Res 2018;28:1747–56.
[35] Hu W, Wang G, Chen Y, Yarmus LB, Liu B, et al. Coupled immune stratification and identification of therapeutic candidates in patients with lung adenocarcinoma. Aging (Albany NY) 2020;12:16514–38.
[36] Hanzelmann S, Castelo R, Guinney J. GSVA: gene set variation analysis for microarray and RNA-seq data. BMC Bioinf 2013;14:7.
[37] Yoshihara K, Shahmoradgoli M, Martinez E, Vegesna R, Kim H, et al. Inferring tumour purity and stromal and immune cell admixture from expression data. Nat Commun 2013;4:2612.
[38] Bindea G, Mlecnik B, Tosolini M, Kirilovsky A, Waldner M, et al. Spatiotemporal dynamics of intratumoral immune cells reveal the immune landscape in human cancer. Immunity 2013;39:782–95.
[39] Yi L, Wu G, Guo L, Zou X, Huang P. Comprehensive analysis of the PD-L1 and immune infiltrates of m(6)A RNA methylation regulators in head and neck squamous cell carcinoma. Mol Ther Nucleic Acids 2020;21:299–314.
[40] Wu M, Wang Y, Liu H, Song J, Ding J. Genomic analysis and clinical implications of immune cell infiltration in gastric cancer. Biosci Rep 2020;40.
[41] Bonneville R, Krook MA, Kautto EA, Miya J, Wing MR, et al. Landscape of microsatellite instability across 39 cancer types. JCO Precis Oncol 2017:2017.
[42] Thorsson V, Gibbs DL, Brown SD, Wolf D, Bortone DS, et al. The immune landscape of cancer. Immunity 2018;48. 812–30 e14.
[43] Jiang P, Gu S, Pan D, Fu J, Sahu A, et al. Signatures of T cell dysfunction and exclusion predict cancer immunotherapy response. Nat Med 2018;24:1550–8.
[44] Wang Q, Li M, Yang M, Yang Y, Song F, et al. Analysis of immune-related signatures of lung adenocarcinoma identified two distinct subtypes: implications for immune checkpoint blockade therapy. Aging (Albany NY) 2020;12:3312–39.
[45] Zack TI, Schumacher SE, Carter SL, Cherniack AD, Saksena G, et al. Pan-cancer patterns of somatic copy number alteration. Nat Genet 2013;45:1134–40.
[46] Nishiyama A, Nakanishi M. Navigating the DNA methylation landscape of cancer. Trends Genet 2021;37:1012–27.
[47] Dvinge H, Git A, Graf S, Salmon-Divon M, Curtis C, et al. The shaping and functional consequences of the microRNA landscape in breast cancer. Nature 2013;497:378–82.
[48] Cuijpers SAG, Vertegaal ACO. Guiding mitotic progression by crosstalk between post-translational modifications. Trends Biochem Sci 2018;43:251–68.
[49] Mendiratta G, Ke E, Aziz M, Liarakos D, Tong M, et al. Cancer gene mutation frequencies for the U.S. population. Nat Commun 2021;12:5961.
[50] Liu Y, Gu W. p53 in ferroptosis regulation: the new weapon for the old guardian. Cell Death Differ 2022.
[51] Jiang L, Kon N, Li T, Wang SJ, Su T, et al. Ferroptosis as a p53-mediated activity during tumour suppression. Nature 2015;520:57–62.
[52] Wang SJ, Li D, Ou Y, Jiang L, Chen Y, et al. Acetylation is crucial for p53-mediated ferroptosis and tumor suppression. Cell Rep 2016;17:366–73.
[53] Jennis M, Kung CP, Basu S, Budina-Kolomets A, Leu JI, et al. An African-specific polymorphism in the TP53 gene impairs p53 tumor suppressor function in a mouse model. Genes Dev 2016;30:918–30.
[54] Tarangelo A, Magtanong L, Bieging-Rolett KT, Li Y, Ye J, et al. p53 Suppresses Metabolic Stress-Induced Ferroptosis in Cancer Cells. Cell Rep 2018;22:569–75.
[55] Xie Y, Zhu S, Song X, Sun X, Fan Y, et al. The Tumor Suppressor p53 Limits Ferroptosis by Blocking DPP4 Activity. Cell Rep 2017;20:1692–704.
[56] Zhou N, Bao J. FerrDb: a manually curated resource for regulators and markers of ferroptosis and ferroptosis-disease associations. Database (Oxford) 2020;2020.
[57] Liu Z, Zhao Q, Zuo ZX, Yuan SQ, Yu K, et al. Systematic analysis of the aberrances and functional implications of ferroptosis in cancer. iScience 2020; 23:101302.
[58] Tang B, Yan R, Zhu J, Cheng S, Kong C, et al. Integrative analysis of the molecular mechanisms, immunological features and immunotherapy response of ferroptosis regulators across 33 cancer types. Int J Biol Sci 2022;18:180–98.
[59] Bai D, Feng H, Yang J, Yin A, Lin X, et al. Genomic analysis uncovers prognostic and immunogenic characteristics of ferroptosis for clear cell renal cell carcinoma. Mol Ther Nucleic Acids 2021;25:186–97.
[60] Mhaidly R, Mechta-Grigoriou F. Role of cancer-associated fibroblast subpopulations in immune infiltration, as a new means of treatment in cancer. Immunol Rev 2021;302:259–72.
[61] Charoentong P, Finotello F, Angelova M, Mayer C, Efremova M, et al. Pan-cancer immunogenomic analyses reveal genotype-immunophenotype relationships and predictors of response to checkpoint blockade. Cell Rep 2017;18:248–62.
[62] Lei G, Zhuang L, Gan B. Targeting ferroptosis as a vulnerability in cancer. Nat Rev Cancer 2022.
[63] Chen X, Kang R, Kroemer G, Tang D. Broadening horizons: the role of ferroptosis in cancer. Nat Rev Clin Oncol 2021;18:280–96.
[64] Zhu H, Liu J, Feng J, Zhang Q, Bian T, et al. Overexpression of TPX2 predicts poor clinical outcome and is associated with immune infiltration in hepatic cell cancer. Medicine (Baltimore) 2020;99:e23554.
[65] Bian T, Zheng M, Jiang D, Liu J, Sun H, et al. Prognostic biomarker TUBA1C is correlated to immune cell infiltration in the tumor microenvironment of lung adenocarcinoma. Cancer Cell Int 2021;21:144.
[66] Zhu H, Hu X, Gu L, Jian Z, Li L, et al. TUBA1C is a prognostic marker in low-grade glioma and correlates with immune cell infiltration in the tumor microenvironment. Front Genet 2021;12:759953.
[67] Cejalvo T, Gargini R, Segura-Collar B, Mata-Martinez P, Herranz B, et al. Immune profiling of gliomas reveals a connection with IDH1/2 mutations, tau function and the vascular phenotype. Cancers (Basel) 2020;12.
[68] Shen H, Wang Z, Ren S, Wang W, Duan L, et al. Prognostic biomarker MITD1 and its correlation with immune infiltrates in hepatocellular carcinoma (HCC). Int Immunopharmacol 2020;81:106222.
[69] Chen C, Sheng Y. Prognostic impact of MITD1 and associates with immune infiltration in kidney renal clear cell carcinoma. Technol Cancer Res Treat 2021; 20:15330338211036233.
[70] Ding J, He X, Wang J, Cao G, Chen S, et al. Integrative analysis of prognostic value and immune infiltration of spindle and kinetochore-associated family members in breast cancer. Bioengineered 2021;12:10905–23.
[71] Yu DC, Chen XY, Li X, Zhou HY, Yu DQ, et al. Transcript levels of spindle and kinetochore-associated complex 1/3 as prognostic biomarkers correlated with immune infiltrates in hepatocellular carcinoma. Sci Rep 2021;11:11165.